THE PROTEIN SOCIETY

Insights into β2-adrenergic receptor binding from structures of the N-terminal lobe of ARRDC3

Shiqian Qi,[1] Morgan O'Hayre,[2] J. Silvio Gutkind,[2] and James H. Hurley[1,3]*

[1]Department of Molecular and Cell Biology and California Institute for Quantitative Biosciences, University of California, Berkeley, Berkeley, California 94720

[2]Oral and Pharyngeal Cancer Branch, National Institute of Dental Research, National Institutes of Health, Bethesda, Maryland 20892

[3]Life Sciences Division, Lawrence Berkeley National Laboratory, Berkeley, California 94720

Received 29 August 2014; Revised 5 September 2014; Accepted 8 September 2014
DOI: 10.1002/pro.2549
Published online 12 September 2014 proteinscience.org

ABSTRACT: ARRDC3 is one of six known human α-arrestins, and has been implicated in the downregulation of the β2-adrenergic receptor (β2AR). ARRDC3 consists of a two-lobed arrestin fold and a C-terminal tail containing two PPYX motifs. In the current model for receptor downregulation by ARRDC3, the arrestin fold portion is thought to bind the receptor, while the PPXY motifs recruit ubiquitin ligases of the NEDD4 family. Here we report the crystal structures of the N-terminal lobe of human ARRDC3 in two conformations, at 1.73 and 2.8 Å resolution, respectively. The structures reveal a large electropositive region that is capable of binding phosphate ions of crystallization. Residues within the basic patch were shown to be important for binding to β2AR, similar to the situation with β-arrestins. This highlights potential parallels in receptor recognition between α- and β-arrestins.

Keywords: protein crystallography; ubiquitin ligase; arrestin; coimmunoprecipitation; asthma

Introduction

Biological signaling cycles consist, at a minimum, of an on switch and an off switch. The off switch is just as critical as the on for biological function. Yet robust "off" responses can frustrate pharmacological interventions that activate natural "on" switches. An example is the treatment of bronchoconstriction in asthma by inhaled β2-adrenergic receptor (β2AR) agonists, where drug efficacy may be limited in part by downregulation of β2AR following treatment. This loss of efficacy following dosing is termed tachyphylaxis. Downregulation is a long-term negative regulatory mechanism that consists of the internalization and proteolytic degradation of a receptor. Often, although not always, the downregulation begins with the sequential activation, phosphorylation, and ubiquitination of the receptor. Ubiquitination may precede or follow endocytosis, and in downregulation, endocytosis is followed by sorting of the receptor to the lysosome, where it is degraded.[1,2]

G-protein coupled receptors (GPCRs)[3] are ubiquitous cell surface receptors and are the largest class of targets for clinically useful drugs. Their deactivation is coordinated by the arrestin and arrestin-related proteins.[4–6] A common fold consisting of two lobes, one N-terminal and one C-terminal, defines the arrestin and arrestin-related class. Each lobe in turn consists of a β sandwich fold. This class consists of the α-arrestins, the β- and visual arrestins, and the VPS26 proteins.[5–7] β- and visual

Additional Supporting Information may be found in the online version of this article.

Coordinates have been deposited with the RCSB with accession codes 4R7V and 4R7X.

James Hurley is the recipient of the Protein Society 2014 Hans Neurath Award.

Grant sponsor: American Asthma Foundation AAF 2011-0228 and NIH Intramural program, NIDCR.

*Correspondence to: James H. Hurley, Dept. of Molecular and Cell Biology, University of California, Berkeley, Berkeley, California 94720. E-mail: jimhurley@berkeley.edu

arrestins have been by far the most extensively studied of the three classes. The β- and visual arrestins are most commonly associated with receptor desensitization,[4] although they have also been implicated in downregulation.[8] Unlike downregulation, desensitization is reversible upon receptor dephosphorylation and retrograde sorting to the plasma membrane. VPS26 proteins are involved in this latter retrograde sorting pathway.[9]

The α-arrestins have come the forefront of attention in recent years for their role as adaptors that direct receptors to their destruction in the lysosomal sorting pathway.[5,10,11] Typically this occurs when PPXY motifs of the α-arrestin recruit a WW domain-containing ubiquitin ligase to the receptor.[7,10–12] Ligase-independent downregulatory functions have also been reported[12] and direct interactions with the ESCRT machinery in lysosomal sorting and shedding microvesicle biogenesis have been proposed.[13,14] The genome of the simple eukaryote *Saccharomyces cerevisiae* encodes 14 α-arrestins, one VPS26 protein, but no β-arrestins. The human proteome appears to contain at least six α-arrestins, ARRDC1–5 and TXNIP. Thus, the role of α-arrestins appears to be ancient, widespread, and fundamental. The relationship between individual α-arrestins and the receptors that they target seems to be complex and partly redundant. ARRDC3 in particular has been directly[15–17] or indirectly[18] implicated in the downregulation of β2AR by multiple lines of evidence in a range of cell types and in mice.

Table I. *Statistics of Crystallographic Data Collection and Refinement*

	ARRDC3(1–165)	ARRDC3(1–180)
Beamline	8.3.1 at ALS	22-ID at APS
Data collection		
Space group	C2	$P4_12_12$
Cell dimension		
a, b, c (Å)	67.55, 36.16, 74.33	107.9, 107.9, 117.8
α, β, γ (°)	90, 107.4, 90	90.0, 90.0, 90.0
Wavelength (Å)	1.11587	1.00000
Resolution (Å)	30.0–1.73 (1.79–1.73)	50.000–2.65 (2.74–2.65)
No. of reflections	17185	21676
Completeness (%)	96.7 (95.6)	98.9 (93)
Redundancy	3.8 (3.8)	5.1 (2.4)
R_{sym} (%)	3.5 (15.1)	19.5 (72.7)
$\langle I \rangle / \langle \sigma(I) \rangle$	21.6 (10.0)	3.7 (0.7)
Refinement		
Resolution (Å)	28.8–1.73 (1.84–1.73)	32.0–2.80 (2.72–2.80)
R_{work}/R_{free} (%)	20.1/23.6 (22.3/25.4)	21.6/25.1 (35.6/40.1)
Average *B*-factor (Å)	39.442	71.529
protein		
R.m.s. deviation from ideality		
Bond length (Å)	0.003	0.002
Bond angle (°)	0.766	0.538
Ramachandran plot		
Favored (%)	96.3	96.82
Allowed (%)	3.7	3.18
Outlier (%)	0	0

This figure also includes an iMolecules 3D interactive version that can be accessed via the link at the bottom of this figure's caption.

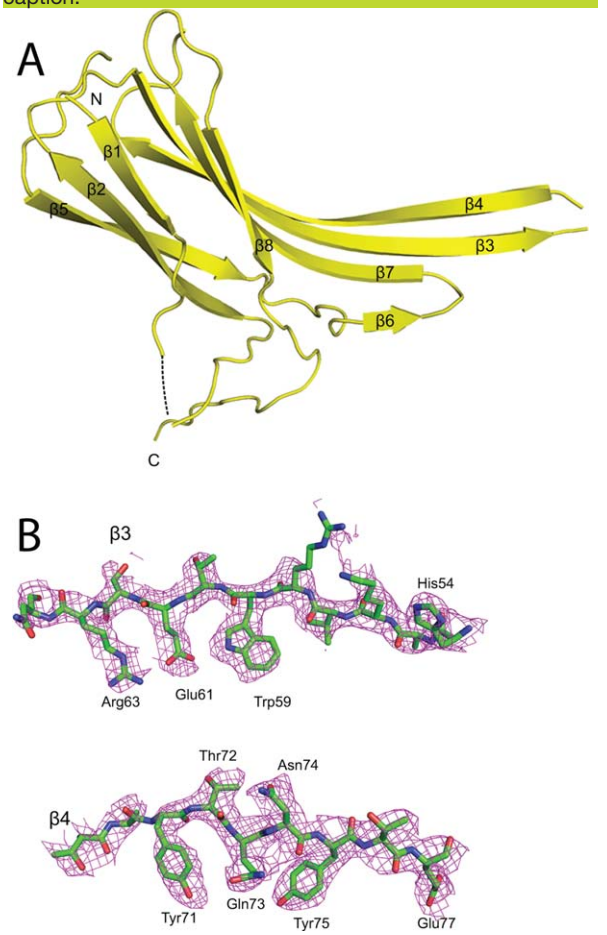

Figure 1. Structure of the N-terminal lobe of ARRDC3 at 1.73 Å. (A) Ribbon model of the overall structure. (B) Fourier $2F_o–F_c$ omit synthesis. An interactive view is available in the electronic version of the article.

Our laboratory has been seeking to understand at the structural and mechanistic biochemical level how ARRDC3 and other ARRDCs might direct the ubiquitination and downregulation of the β2AR and other GPCRs.[19] This information might prove important in designing downregulation antagonists that could inhibit tachyphylaxis (loss of response) to receptor agonists used to treat asthma and other conditions. Currently, there is a void of information on how α-arrestins might bind to GPCRs. The structure of a vasopressin receptor phosphopeptide bound to β-arrestin-1[20] recently showed that, at least for this β-arrestin, all of the binding determinants are encoded in the N-terminal lobe of the arrestin fold. Reasoning that the N-terminal lobe of ARRDC3 might, by analogy with β-arrestin-1, be the locus for receptor binding, we determined its crystal structure. The

This figure also includes an iMolecules 3D interactive version that can be accessed via the link at the bottom of this figure's caption.

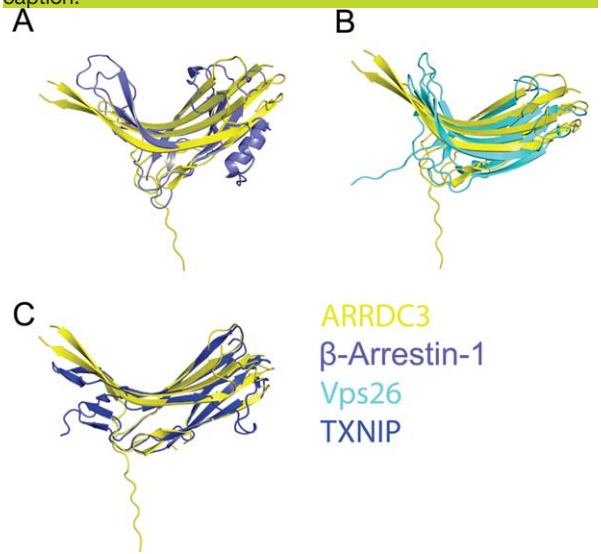

Figure 2. Comparison of ARRDC3 to other arrestin fold proteins. Superposition with (A) β-arrestin-1, (B) Vps26, and (C) TXNIP, respectively. The molecules are colored yellow, light blue, cyan, and blue, respectively. An interactive view is available in the electronic version of the article.

structure was used to infer the role of a cluster of basic residues on the concave face of the N-terminal lobe (N-lobe for short) in receptor binding.

Results

Structure of the N-lobe of ARRDC3

A construct spanning residues 1–165 of human ARRDC3, along with vector-derived residues Leu-Glu-His_6, was crystallized in space group *C*2, with one molecule per asymmetric unit [Table I; Fig. 1(A,B)]. The structure was determined to 1.73 Å resolution by molecular replacement with the N-lobe of TXNIP.[21] The structure is essentially a core arrestin β-sandwich, stripped to essentials [Fig. 1(A)]. The sandwich consists of one three- and one four-stranded β-sheet, which respectively contain strands 1, 2, and 5, and strands 3, 4, 7, and 8. The only embellishment to the minimal pattern is that strand 8 ends before the rest of the sheet, and the short strand 6 takes its place in partnering with strand 7. Neither the two small two-stranded sheets of the N-lobe of TXNIP, nor the single α-helix of β-arrestin, are present.

The lobes of the arrestin fold proteins are typically highly curved, thus most of their surface is part of either a concave or a convex face. Compared to other available structures of arrestin superfamily proteins, this structure of the N-lobe ARRDC3 is flatter than those of the visual and β-arrestins[22,23] [Fig. 2(A)] and VPS26[24] [Fig. 2(B)], but similar to

This figure also includes an iMolecules 3D interactive version that can be accessed via the link at the bottom of this figure's caption.

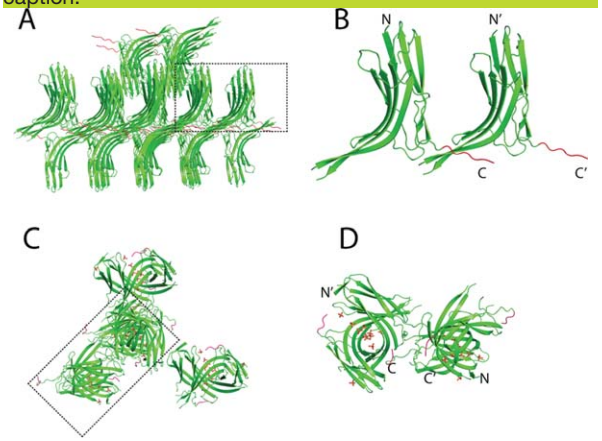

Figure 3. Lattice interactions occur primarily via the C-terminus. (A) The overall packing of ARRDC3(1–165) molecules in the crystal. (B) A close-up with the C-terminal vector-derived residues highlighted in red. (C) The overall packing of ARRDC3(1–180) molecules in crystal. (D) A close-up of the lattice dimers in the 1–180 crystal. An interactive view is available in the electronic version of the article.

that of TXNIP[21,25] [Fig. 2(C)]. This stems mainly from a less curved conformation for the β3–β4 pair in this structure, which are the two longest strands. The conformation of the β3–β4 pair is inter-related to the crystal packing in this structure. The lattice [Fig. 3(A)] is held together primarily by the formation of a three-stranded β-sheet by a pairing in trans between the internally unpaired edge of β4 and the C-terminal portion of the construct (residues 162–165 and the first five vector-derived residues), which projects away from the rest of the molecule [Fig. 3(B)]. This indicates that, at least in the absence of ligands, the N-lobe of ARRDC3 is capable of adopting an unusually flat shape.

Structure of the N-lobe bound to phosphate ions

A second crystal form of the ARRDC3 N-lobe was obtained, this time using a construct spanning residues 1–180. This protein was crystallized from a high phosphate buffer in space group $P4_12_12$ with two molecules in the asymmetric unit [Table I; Fig. 3(C,D)]. The structure was solved to 2.80 Å resolution using as a search model the 1.73 Å structure described above. Residues beyond 168 are disordered in the structure.

In this structure, the N-lobe adopts the highly curved shape characteristic of the arrestin family [Fig. 4(A,B)]. The two molecules in the asymmetric unit wrap themselves about one another and about a central channel containing at least ten ordered phosphate ions in close proximity to one another

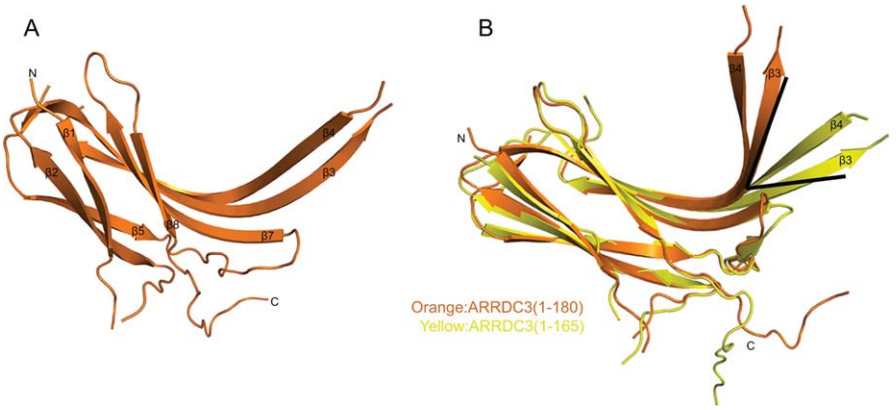

Figure 4. Structure of a curved conformation of ARRDC3 at 2.8 Å resolution. (A) The overall structure of ARRDC3(1–180). (B) Superposition of the two structures shows that β3 and β4 bend by about 45° compared to the 1–165 structure. ARRDC3(1–180) and 1–165 are colored as orange and yellow respectively.

[Fig. 5(A–E)]. Basic residues that are contributed by the concave faces of both molecules line the central channel. These residues include Lys45, Lys48, His50, Lys52, His54, Lys56, Arg58, Lys85, Arg135, Lys139, His143, and Lys151 [Fig. 5(B–E)]. This leads to an exceptionally electropositive character

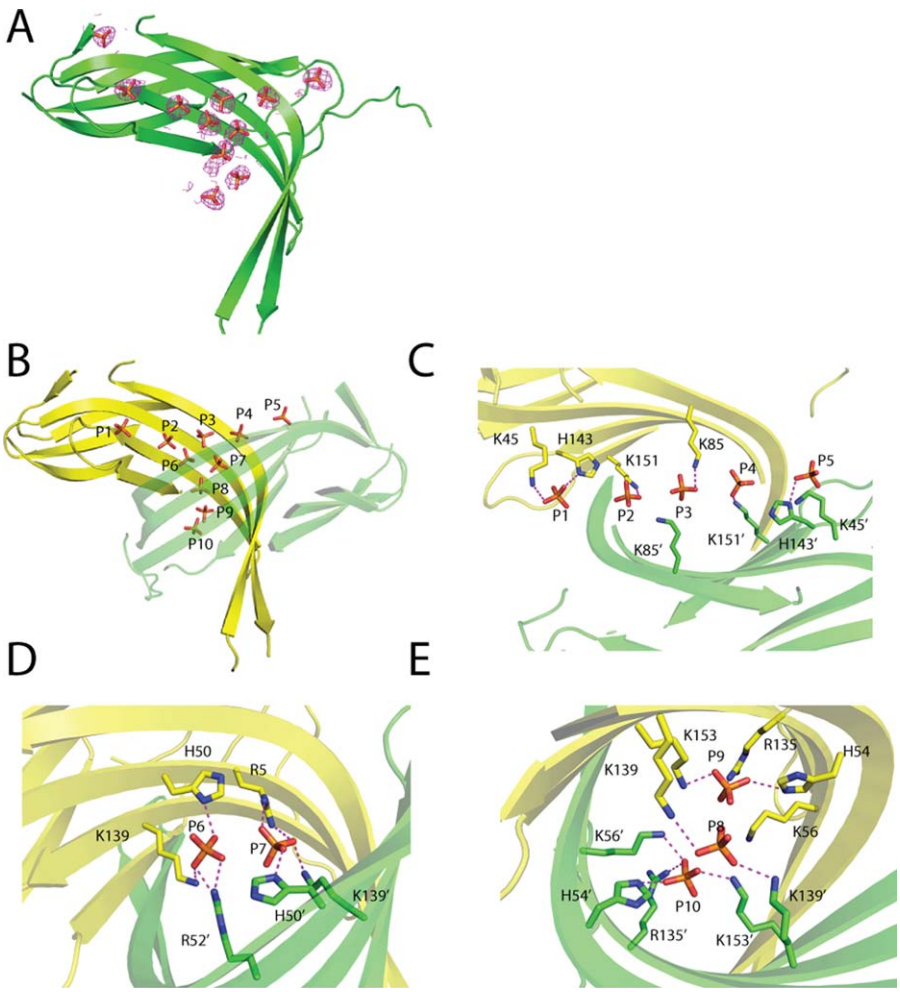

Figure 5. Bound phosphates of crystallization. Overall view of all of the phosphates belonging to one asymmetric unit of ARRDC3(1–180) are shown with one of the two copies of the protein in the background. The density is from an F_o–F_c omit synthesis contoured at 2.0σ with the phosphate ions removed. Density is displayed within a 3.0 Å radius of any atom of a phosphate group. (B–E) Detail of the hydrogen bonds between phosphate groups and the ARRDC3(1–180) dimer. The phosphate groups are labeled P1 to P10 and colored orange. Molecule A is yellow while molecule B is green.

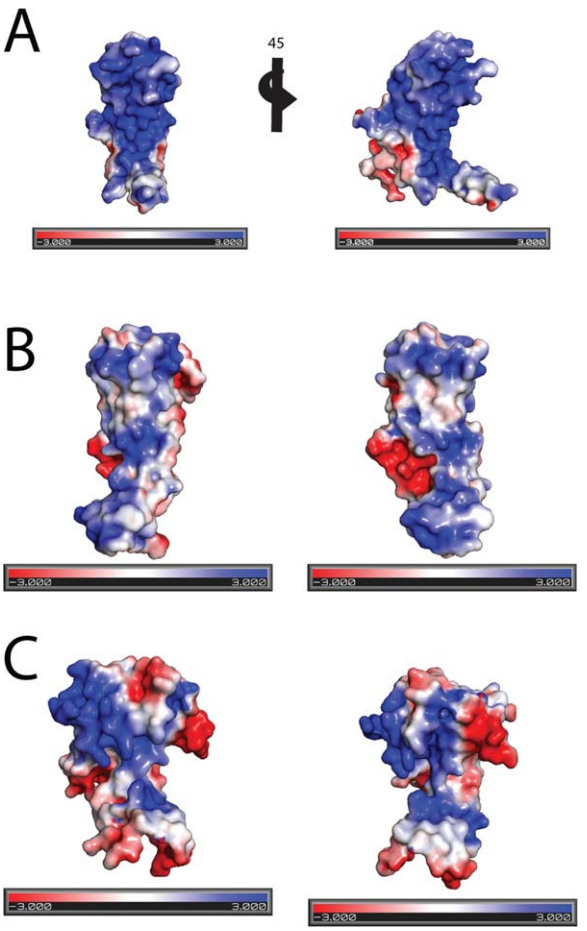

Figure 6. Electrostatic properties of ARRDC3 and N-lobes of other arrestin fold proteins. Surfaces of (A) ARRDC3(1–180), (B) TXNIP, and (C) β-arrestin-1. Color bars are scaled in units of kT/e.

for the surface of ARRDC3 in this region [Fig. 6(A)].

The most similar available structure, that of TXNIP, is electrically neutral in the region of its concave face [Fig. 6(B)]. Most of the basic residues noted above are replaced by hydrophobic or acidic residues in TXNIP (Fig. 7), accounting for the difference in electrical polarization. The N-lobe of β-arrestin-1 is, like ARRDC3, electropositive [Fig. 6(C)]. In the crystal structure of the β-arrestin-1:vasopressin tail phosphopeptide complex, the N-terminal part of the phosphopeptide spanning residues 347–353 is bound in this general region [Fig. 8(A,B)]. However, there is little similarity in detail. In the overlaid structures, one of the phosphate ions is within 6 Å of the position of VR pThr347, while the others are farther [Fig. 8(A)]. The C-terminal part (354–367) of the vasopressin tail peptide binds mainly to the N-terminal β strand and the single helix α-helix of β-arrestin-1, which are both absent in ARRDC3 [Fig. 8(A)]. Thus, while the N-lobes of β-arrestin-1 and ARRDC3 share a common capacity for binding a large number of phosphate groups, the precise positioning of the sites is different. They highlight that these proteins are similar in the most general terms, but must differ considerably in the molecular details of receptor binding.

Basic clusters are involved in receptor binding in cells

Given the striking clustering of phosphate ions in the groove formed by the concave face of the N-lobe, and the analogy to the VR: β-arrestin-1 structure, we sought to test whether the basic face of the N-lobe of ARRDC3 was important for receptor recognition. Residues directly involved in phosphate binding were mutated (Lys48, Lys52, Lys56, Arg58, Lys85, Arg135, Lys139) together with others nearby or in regions equivalent to pSer/Thr binding sites in the VR: β-arrestin-1 structure (Arg33, Lys43, Lys153) and elsewhere (Lys5, Lys7, Arg109, Arg144). The following mutations were made, each targeting one continuous basic patch on the surface [Fig. 9(A,B)]: M1: K7E/R33E/R109E, M2: K5E/K43E/R144E, M3: K56E/R58E/R135E/K153E, and M4: K48E/R52E/K85E/K139E. Mutants M1 and M2 cover parts of the surface not involved in binding phosphates of crystallization; M3 is primarily and M4 entirely comprised of phosphate-interacting residues.

HEK293 cells stably expressing FLAG-β2AR were prepared by lentiviral transduction, and expression was verified by flow cytometry (Supporting Information Fig. S1). The stably transduced HEK293 FLAG-β2AR cells were used to assay for co-immunoprecipitation with wild type (WT) YFP-ARRDC3 and with four variants encoding the mutants M1–M4 described above. A robust interaction between FLAG- β2AR and YFP-ARRDC3 WT was observed by co-IP. Co-IP was disrupted by mutations of lysine and arginine residues, to a greater extent in M3 and M4 as compared to M1 and M2 [Fig. 9(C)]. Specifically, the binding to FLAG-β2AR was abolished in the M4 mutant, indicating that other basic patches contribute to the binding of ARRDC3 to β2AR, but the basic residues depicted in Figure 9(A) and (B) in the context of the M4 mutation define a surface area that is strictly required for the association of ARRDC3 with β2AR. Collectively, these data support that the electropositive surface of ARRDC3, and in particular the portion involved in binding phosphate ions of crystallization, is important for its interaction with β2AR.

Discussion

The two structures determined here confirm the membership of ARRDC3 in the arrestin fold family. Human ARRDC3 has sequence identity of 42 and 19% with human TXNIP and β-arrestin-1, respectively. In terms of its overall fold, the N-terminal lobe of ARRDC3 could be considered a stripped-

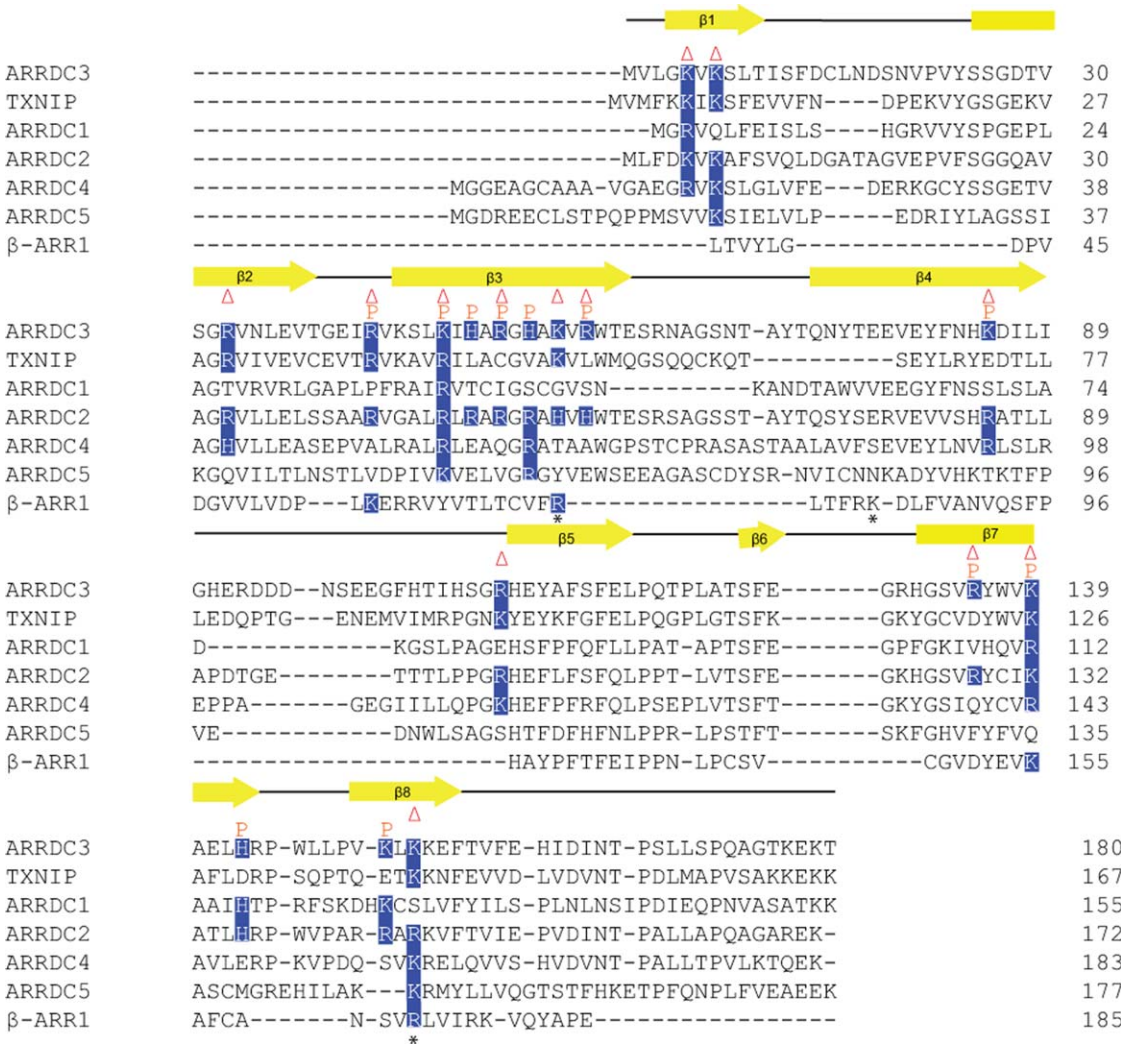

Figure 7. Structure-based alignment of N-terminal lobes of ARRDCs and β-arrestin-1. A three-dimensional alignment of ARRDC3, TXNIP, and β-arrestin-1 was generated first. A multiple sequence alignment of other ARRDCs was then generated and aligned with respect to the overlaid structures. The sequence of β-arrestin-1 is shown only for the subset of residues that could be aligned with the ARRDCs. The secondary structure of ARRDC3 is show at the top of the alignment. Basic residues involved in the electropositive surface are highlight with a blue background. "Δ" on the top means that these residues had been mutated to Glu for the functional assay shown in Figure 9. "*P*" on top of sequence stands for the residues that interact with phosphate groups. "*" at the bottom of sequence shows the residues of β-arrestin-1 that interact with the vasopressin tail peptide complex structure.[20]

down version on TXNIP. Whilst missing two small β-sheets found in TXNIP, the core β sandwich is largely superimposable. Despite the close similarity in overall fold, key Cys residues of TXNIP are not present in ARRDC3, and it is not clear whether their similar folds are used for common functions.

It is not surprising that the three-dimensional structure is more distant from that of β-arrestin-1 given that the pairwise sequence identity is in the twilight zone of significance. The electropositive surface character of ARRDC3 is nevertheless more similar to that of β-arrestin-1 than it is to the neutral surface of TXNIP. This likely related to the common function of ARRDC3 and β-arrestin-1 in regulating the internalization and inactivation of receptors that are subject to phosphoregulation.

Inspired by the finding that the main binding site on β-arrestin-1 for a phosphopeptide from the vasopressin receptor was found on the highly basic concave surface of the N-terminal lobe,[20] we tested the function of the equivalent region on ARRDC3. As assessed by coimmunoprecipitation from cell culture, this region is essential for the interaction between ARRDC3 and β2AR. We have not, however, been able to demonstrate direct binding between the ARRDC3 N-terminal domain and purified β2AR. It is therefore currently uncertain whether the interaction between the ARRDC3 N-terminal domain and β2AR is direct or indirect. The exceptionally basic character of the ARRDC3 concave surface does suggest that the ligands for ARRDC3 are likely to be highly negatively charged, most likely as a result of phosphorylation.

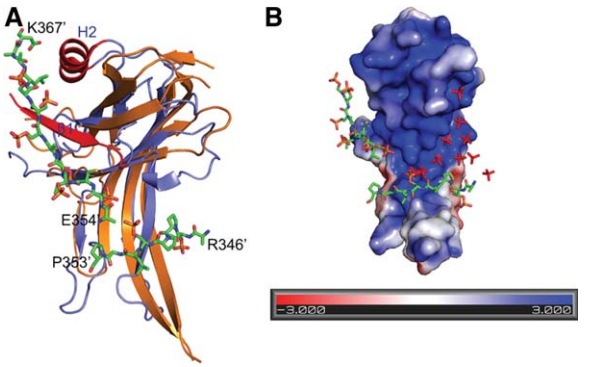

Figure 8. Speculative model for receptor phosphopeptide binding to ARRDC3. (A) The vasopressin phosphopeptide from 1JQI[20] was docked onto the structure of ARRDC3(1–180) by overlaying the backbones of the two N-terminal lobes. This model indicates that the N-terminal of the phosphate tail of β-2AR might interact with ARRDC3 N-lobe in a similar mode to β-arrestin-1, insofar as the electrostatic properties are conserved and there are not extensive steric overlaps. The C-terminal of phosphate peptide probably cannot bind in the same way since β1 and α1 of β-arrestin-1 do not have counterparts in ARRDC3. ARRDC3 is colored orange while β-arrestin-1 is colored light blue. The unique β1 and α1 of β-arrestin-1 are colored red. The phosphate peptide is colored green. (B) Electrostatic surface representation of ARRDC3 with the peptide from (A) shown and bound phosphate ions for comparison.

This point will be important for understanding how ARRDC3 downregulates the β2AR, and may help clarify whether ARRDC3 is a promising target for inhibitors of β2AR agonist tachyphylaxis.

Materials and Methods

Cloning and protein purification

DNAs coding for residues 1–165 and 1–180 of human ARRDC3 were subcloned into pHis-parallel$_2$[26] for expression with TEV cleavable C- and N-terminal His$_6$ tags, respectively. These constructs were expressed in *E. coli* BL21-gold (DE3) cell (Agilent Technologies). IPTG was added when the OD_{600} reached 1.0. After incubation with 0.2 m*M* IPTG overnight at 18°C, the cells were pelleted with centrifugation at 4000*g* for 10 min. Cell pellets were lysed in 25 m*M* Tris–HCl pH 8.0, 150 m*M* NaCl, 0.5 m*M* TCEP–HCl, and 1 m*M* PMSF. The lysate was centrifuged at 25,000*g* for 1 h at 4°C. The supernatant was purified on Ni-NTA resin, followed by a Hi Trap Q HP column. For 1–180 construct, peak fractions were pooled and digested by TEV protease overnight at 4°C. His$_6$-TEV was removed by incubating with Ni-NTA resin for 0.5 h. The sample was then applied to a Superdex 200 16/60 column equilibrated with 150 m*M* NaCl, 25 m*M* Tris–HCl 8.0. For the 1–165 construct, peak fractions from the Hi Trap Q HP column were directly loaded onto the Superdex 200 16/60 column. The Superdex 200 peaks were pooled and flash frozen in liquid N_2.

Crystallization of the N-terminal Domain of ARRDC3

Purified proteins were concentrated to 10 mg/mL with a 10 kDa cutoff centrifugal filter (Millipore). Crystals were grown by the hanging-drop vapor-

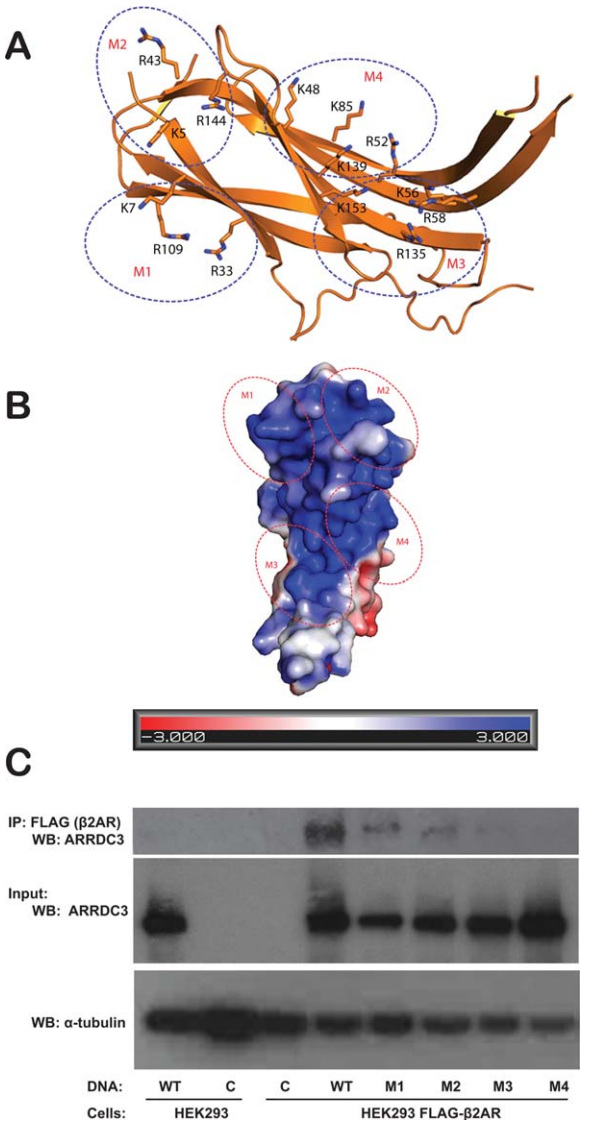

Figure 9. Mutational analysis of the basic surface. (A) Residues were selected for mutation in four clusters and are mapped onto the structure in the phosphate-bound conformation. (B) Clusters of basic residues correspond to four patches that cover the basic surface of the N-terminal lobe. Saturating color is at ±3.0 kT/e. (C) A co-IP assay was performed by transfecting HEK293-FLAG-B2AR cells with WT YFP-ARRDC3 and mutant YFP-ARRDC3 plasmids (M1–M4, corresponding to M1: K7E/R33E/R109E, M2: K5E/K43E/R144E, M3: K56E/R58E/R135E/K153E, and M4: K48E/R52E/K85E/K139E) or vector control (C). HEK293 cells lacking FLAG-β2AR were transfected with YFP-ARRDC3 WT or vector control (C) and used as a control for nonspecific interactions. Lysates were immunoprecipitated with anti-FLAG affinity beads and probed for ARRDC3, and whole cell lysate (input) was probed with α-tubulin or ARRDC3 antibodies as controls for loading and expression.

diffusion method at 21°C. The 1–180 protein was mixed with well buffer composed of 0.75*M* $NH_4H_2PO_4$, 0.1*M* sodium citrate, 3.0% (w/v) 6-aminohexanoic acid at a 1:1 ratio. Crystals appeared with 24 h and grew to full size after 5 days. Crystals were flash-frozen with liquid N_2 in a cryo-protectant solution of 20% (v/v) glycerol, 0.75*M* $NH_4H_2PO_4$, 0.1*M* sodium citrate. The 1–165 protein was crystallized in 20% (w/v) PEG 3350, 0.1 M Tris–HCl 7.0, 0.2*M* $(NH_4)_2SO_4$, 50 m*M* guanidine–HCl. Crystals appeared within 1 week and reached full size after 21 days. The crystals were flash-frozen with liquid N_2 in 20% (v/v) glycerol, 20% (w/v) PEG 3350, 0.1*M* Tris–HCl 7.0, 0.2*M* $(NH_4)_2SO_4$, 50 m*M* guanidine–HCl.

Data collection and structure determination

Diffraction data for 1–180 and 1–165 were collected at APS beamline 22-ID and ALS beamline 8.3.1, respectively. A full data set from one single crystal was processed with HKL2000 (HKL Research). Data collection and processing statistics are given in Table I. The structure of the construct of 1–165 was solved by the molecular replacement method with Phaser[27] using the structure of the N-terminal lobe of TXNIP (4GFX)[21] as a search model. Model building and refinement were finished with ARP/wARP,[28] Coot,[29] Refmac5,[30] and Phenix.[31] The structure of 1–180 was solved by molecular replacement method with PHASER using the structure of 1–165 as the search model.

Immunoprecipitation

The pCR3.1 YFP-ARRDC3 plasmid was kindly provided by Dr. Martin-Serrano (King's College). FLAG-β2AR was cloned into the pLESIP lentiviral expression vector. Lentivirus of FLAG-β2AR was prepared by transfection of HEK293t/17 cells with pLESIP FLAG-β2AR, psPAX2, and VSV-G in a 3:2:1 ratio using Turbofect transfection reagent (Thermo Scientific) and 48 and 72 h viral supernatants were collected. HEK293 cells were transduced by infection with 0.45 μm PVDF-filtered FLAG-β2AR lentivirus with 6 μg/ml of polybrene and then selected with 1 μg/mL puromycin (Invitrogen) to generate a stable line. Expression of FLAG-β2AR in HEK293 cells was verified by flow cytometry using a FLAG-PE conjugated antibody (Prozyme) and analyzed on a FACSCalibur (BD Biosciences). Mutations in the pCR3.1 YFP-ARRDC3 plasmid were prepared by site-directed mutagenesis (QuikChange Lightning Multi, Agilent) and confirmed by DNA sequence analysis (NIDCR shared resource facility). Mutation combinations included M1: K7E/R33E/R109E, M2: K5E/K43E/R144E, M3: K56E/R58E/R135E/K153E, and M4: K48E/R52E/K85E/K139E.

For co-immunoprecipitation assays, approximately 2 μg of YFP-ARRDC3 plasmid was transfected into the stable HEK293-FLAG β2AR cells (or normal HEK293 control cells) in 6-well plates using lipofectamine 2000 (Invitrogen). Due to stronger expression of WT ARRDC3 and M4 mutant compared to the M1, M2 and M3 mutants, amounts of plasmid transfected were appropriately adjusted to result in similar expression levels in order to compare levels of co-immunoprecipitation with FLAG-β2AR. After 48 h after transfection, cells were harvested with 300 μL lysis buffer comprised 50 m*M* Tris–HCl (pH7.5), 100 m*M* NaCl, and 1% Triton X-100 and clarified for 10 min at 15,000*g* at 4°C. A fraction of lysate (50 μL) was saved for input lysate and the remaining lysate was used for immunoprecipitation with anti-FLAG M2 affinity beads (Sigma) and rotated for 3 h at 4°C. Beads were washed three times with tris buffered saline (TBS) and eluted with sample buffer and boiled for 5 min. Lysates were run on 10% SDS-PAGE gels for western blot analysis. ARRDC3 antibody was obtained from Abcam (Cambridge, MA) and α-tubulin antibody was from Cell Signaling Technologies (Beverly, MA).

ACKNOWLEDGMENTS

X. Ren is thanked for experimental advice. This work was supported by the American Asthma Foundation (JHH and JSG) and the intramural program of the NIDCR, NIH (JSG). Crystallographic data were collected at Beamline 8.3.1, the Advanced Light Source, Lawrence Berkeley National Laboratory, and at Southeast Regional Collaborative Access Team 22-ID and 22-BM beamlines at the Advanced Photon Source, Argonne National Laboratory. Use of the Advanced Photon Source was supported by the U.S. Department of Energy, Office of Science, Office of Basic Energy Sciences, under Contract No. W-31–109-Eng-38 and was supported by the U.S. DOE under Contract No. DE-AC02-06CH11357. The authors have no conflicts of interest.

REFERENCES

1. Sorkin A, von Zastrow M (2009) Endocytosis and signalling: intertwining molecular networks. Nat Rev Mol Cell Biol 10:609–622.
2. Hislop JN, von Zastrow M (2011) Role of ubiquitination in endocytic trafficking of G-protein-coupled receptors. Traffic 12:137–148.
3. Pierce KL, Premont RT, Lefkowitz RJ (2002) Seven-transmembrane receptors. Nat Rev Mol Cell Biol 3: 639–650.
4. Lefkowitz RJ, Whalen EJ (2004) Beta-arrestins: traffic cops of cell signaling. Curr Opin Cell Biol 16:162–168.
5. Alvarez CE (2008) On the origins of arrestin and rhodopsin. BMC Evol Biol 8:222.
6. Kang DS, Tian XF, Benovic JL (2014) Role of beta-arrestins and arrestin domain-containing proteins in G protein-coupled receptor trafficking. Curr Opin Cell Biol 27:63–71.

7. Patwari P, Lee RT (2012) An expanded family of arrestins regulate metabolism. Trends Endocrinol Metab 23: 216–222.
8. Malik R, Marchese A (2010) Arrestin-2 interacts with the endosomal sorting complex required for transport machinery to modulate endosomal sorting of CXCR4. Mol Biol Cell 21:2529–2541.
9. Bonifacino JS, Hurley JH (2008) Retromer. Curr Opin Cell Biol 20:427–436.
10. Lin CH, MacGum JA, Chu T, Stefan CJ, Emr SD (2008) Arrestin-related ubiquitin-ligase adaptors regulate endocytosis and protein turnover at the cell surface. Cell 135:714–725.
11. Nikko E, Pelham HRB (2009) Arrestin-mediated endocytosis of yeast plasma membrane transporters. Traffic 10:1856–1867.
12. Alvaro CG, O'Donnell AF, Prosser DC, Augustine AA, Goldman A, Brodsky JL, Cyert MS, Wendland B, Thorner J (2014) Specific alpha-arrestins negatively regulate *Saccharomyces cerevisiae* pheromone response by down-modulating the G-protein-coupled receptor Ste2. Mol Cell Biol 34:2660–2681.
13. Rauch S, Martin-Serrano J (2010) Multiple interactions between the ESCRT machinery and arrestin-related proteins: implications in PPXY-dependent budding. J Virol 85:3546–3556.
14. Nabhan JF, Hu R, Oh RS, Cohen SN, Lu Q (2012) Formation and release of arrestin domain-containing protein 1-mediated microvesicles (ARMMs) at plasma membrane by recruitment of TSG101 protein. Proc Natl Acad Sci USA 109:4146–4151.
15. Nabhan JF, Pan H, Lu QA (2010) Arrestin domain-containing protein 3 recruits the NEDD4 E3 ligase to mediate ubiquitination of the beta 2-adrenergic receptor. EMBO Rep 11:605–611.
16. Patwari P, Emilsson V, Schadt EE, Chutkow WA, Lee S, Marsili A, Zhang Y, Dobrin R, Cohen DE, Larsen PR, Zavacki AM, Fong LG, Young SG, Lee RT (2011) The arrestin domain-containing 3 protein regulates body mass and energy expenditure. Cell Metabolism 14:671–683.
17. Shea FF, Rowell JL, Li YCW, Chang TH, Alvarez CE (2012) Mammalian alpha arrestins link activated seven transmembrane receptors to Nedd4 family E3 ubiquitin ligases and interact with beta arrestins. PLoS One 7(12):e50557. doi: 10.1371/journal.pone.0050557.
18. Han SO, Kommaddi RP, Shenoy SK (2013) Distinct roles for beta-arrestin2 and arrestin-domain-containing proteins in beta2 adrenergic receptor trafficking. EMBO Rep 14:164–171.
19. Qi SQ, O'Hayre M, Gutkind JS, Hurley JH (2014) Structural and biochemical basis for ubiquitin ligase recruitment by arrestin-related domain-containing protein-3 (ARRDC3). J Biol Chem 289: 4743–4752.
20. Shukla AK, Manglik A, Kruse AC, Xiao K, Reis RI, Tseng W-C, Staus DP, Hilger D, Uysal S, Huang L-Y, Paduch M, Tripathi-Shukla P, Koide A, Koide S, Weis WI, Kossiakoff AA, Kobilka BK, Lefkowitz RJ (2013) Structure of active beta-arrestin-1 bound to a G-protein-coupled receptor phosphopeptide. Nature 497: 137–141.
21. Polekhina G, Ascher DB, Kok SF, Beckham S, Wilce M, Waltham M (2013) Structure of the N-terminal domain of human thioredoxin-interacting protein. Acta Cryst D 69:333–344.
22. Granzin J, Wilden U, Choe HW, Labahn J, Krafft B, Buldt G (1998) X-ray crystal structure of arrestin from bovine rod outer segments. Nature 391:918–921.
23. Hirsch JA, Schubert C, Gurevich VV, Sigler PB (1999) The 2.8 angstrom crystal structure of visual arrestin: a model for arrestin's regulation. Cell 97:257–269.
24. Shi H, Rojas R, Bonifacino JS, Hurley JH (2006) The retromer subunit Vps26 has an arrestin fold and binds Vps35 through its C-terminal domain. Nat Struct Mol Biol 13:540–548.
25. Hwang J, Suh H-W, Jeon YH, Hwang E, Nguyen LT, Yeom J, Lee S-G, Lee C, Kim KJ, Kang BS, Jeong J-O, Oh T-K, Choi I, Lee J-O, Kim MH (2014) The structural basis for the negative regulation of thioredoxin by thioredoxin-interacting protein. Nat Commun 5:10–23.
26. Sheffield P, Garrard S, Derewenda Z (1999) Overcoming expression and purification problems of RhoGDI using a family of "parallel" expression vectors. Protein Expr Purif 15:34–39.
27. McCoy AJ, Grosse-Kunstleve RW, Adams PD, Winn MD, Storoni LC, Read RJ (2007) Phaser crystallographic software. J Appl Cryst 40:658–674.
28. Langer G, Cohen SX, Lamzin VS, Perrakis A (2008) Automated macromolecular model building for X-ray crystallography using ARP/wARP version 7. Nat Protoc 3:1171–1179.
29. Emsley P, Lohkamp B, Scott WG, Cowtan K (2010) Features and development of Coot. Acta Cryst D 66: 486–501.
30. CCP4 (1994) The CCP4 suite: programs for protein crystallography. Acta Cryst A 50:760–763.
31. Adams PD, Afonine PV, Bunkoczi G, Chen VB, Davis IW, Echols N, Headd JJ, Hung LW, Kapral GJ, Grosse-Kunstleve RW, McCoy AJ, Moriarty NW, Oeffner R, Read RJ, Richardson DC, Richardson JS, Terwilliger TC, Zwart PH (2010) PHENIX: a comprehensive Python-based system for macromolecular structure solution. Acta Cryst D 66:213–221.